Thermal modeling of evacuated tubes-solar air collectors

Pierre-Luc Paradis*[a], Daniel R. Rousse[b], Stéphane Hallé[c], Louis Lamarche[d], Guillermo Quesada[e]

*corresponding author

[a] Industrial Research Chair in Energy Technologies and Energy Efficiency (t3e),
École de technologie supérieure, Université du Québec, Montréal, Canada
1100, rue Notre-Dame Ouest
Montréal (Québec) H3C 1K3
514 396-8800 # 7503
pierre-luc@t3e.info

[b] Industrial Research Chair in Energy Technologies and Energy Efficiency (t3e),
École de technologie supérieure, Université du Québec, Montréal, Canada
1100, rue Notre-Dame Ouest
Montréal (Québec) H3C 1K3
daniel@t3e.info

[c] École de technologie supérieure, Université du Québec, Montréal, Canada
1100, rue Notre-Dame Ouest
Montréal (Québec) H3C 1K3
stephane.halle@etsmtl.ca

[d] École de technologie supérieure, Université du Québec, Montréal, Canada
1100, rue Notre-Dame Ouest
Montréal (Québec) H3C 1K3
louis.lamarche@etsmtl.ca

[e] Industrial Research Chair in Energy Technologies and Energy Efficiency (t3e),
École de technologie supérieure, Université du Québec, Montréal, Canada
1100, rue Notre-Dame Ouest
Montréal (Québec) H3C 1K3
guillermo@t3e.info

ABSTRACT

This paper presents a one dimensional thermal model of a solar evacuated tube open at both ends under transient conditions. Variations of fluid mass flow rate, ambient temperature, solar radiation, and wind speed are accounted for. The semi-analytical model relies on energy conservation equation for small control volumes along longitudinal axis of the tube. The first order differential equations obtained for each control volume are solved by use of a fully explicit scheme using a fourth order Runge-Kutta algorithm. An experimental setup has been designed, built and validated in order to assess the predictions provided by the model. The comparison between simulated and experimentally measured outlet air temperature showed a good agreement: a root mean square error on the outlet air temperature of about 0.52 °C and a mean bias difference of 0.20 °C were observed for experiments conducted on a bright sunny day. Finally, the validated model applied for steady state heat transfer is used to conduct an analysis on different parameters. Then, the influence of the environmental parameters (solar radiation, ambient temperature and wind speed) and the operating condition (airflow) is investigated on different performance indicators like the outlet air temperature, the efficiency, the mean convective heat transfer coefficient and the pressure drop. It appeared that the influence of wind and ambient temperature is of minor importance although the influence of solar radiation on the outlet air temperature is significant. Finally, the airflow is the most important parameter acting on the defined performance indicators. Higher is the airflow, better is the efficiency and lower is the outlet air temperature. On the other side, a low airflow can conduct to as much as 100 °C of temperature gain, but the efficiency is then reduced to value as low as 45 %.

Keywords: solar collector, evacuated tube, solar thermal, air.

NOMENCLATURE

D	Tube outside diameter [m]
d	Glass tube thickness [m]
L	Tube length [m]
m	Mass [kg]
c_p	Specific heat [J/kg K]
n	Number of nodes [-]
$\dot{V}$	Volumetric airflow rate[m^3/s]
u	Air velocity [m/s]
$\dot{m}$	Mass airflow rate [kg/s]
G_T	Total tilted solar radiation normal to the plane of the collector [W/m^2]
G	Total horizontal solar radiation [W/m^2]
G_r	Reflected solar radiation [W/m^2]
R	Thermal resistance [K/W]
T	Temperature [°C]
j	Node along the tube axis [-]
i	Time step [-]
P	Pressure [Pa]
Re	Reynolds number
Nu	Nusselt number
$\dot{Q}$	Thermal power transferred to the fluid
A	Projected surface area [m^2]
Greek symbols	
τ	Transmissivity of the glass [-]
α	Absorptivity of the absorber [-]
ρ	Density [kg/m^3]
ε	Emissivity [-]
η	Efficiency [%]
Subscripts	
g	Glass
r	Receiver tube / absorber tube (inner tube)
c	Cover tube (outer tube)
f	Fluid (air)
a	Ambient
in	Inner tube
out	Outer tube
conv	Convection heat transfer
ray	Radiative heat transfer
dyn	Dynamic pressure
useful	Useful
inlet	Tube inlet
outlet	Tube outlet
Abbreviations	
SRCC	Solar Rating Certification Corporation
c.v.	Control volume
CFL	Courant–Friedrichs–Lewy condition for stability of the resolution algorithm

1. INTRODUCTION

In Canada, more than 50 % of the energy consumption in residential, institutional and commercial sectors is related to space heating and domestic hot water [1]. Furthermore, in Quebec where most of the electricity is produced by hydro power available at low cost, a large part of this heat (low quality energy) is produced with electricity (high quality energy). Despite that hydro power is a renewable source of energy, use of high grade energy to produce low temperature heat for domestic hot water and space heating is wasteful. Instead, this heat could be produced with solar thermal collectors with a high level of efficiency. Several different solar collectors are available on the market. Most of them use liquid heat transfer fluid to transfer the heat from the solar collector to a heat storage tank. However there are few difficulties associated with the installation of solar thermal technology in cold climates as in Canada. In fact, glycol is usually used to protect piping against bursting in winter. However, large differences between summer and winter temperatures bring problems of overheating that could cause glycol degradation. Since glycol replacement is expensive, this problem prohibitively extends payback periods for a solar thermal system. A study of Energy Technology Laboratory of Hydro-Québec carried out on 23 solar domestic water heater installed in Quebec concluded that the average payback time is more than 75 years due in part, to the replacement of the glycol that should be done almost every year [2].

In order to bring a solution to this problem, air could be used as the heat transfer fluid instead of water. Using air, freezing and overheating problems are avoided. Furthermore, air is free, could be used in an open loop system and presents no risk of contamination in case of leakage of the piping. Of course, the heat capacity of air is low compared to that of liquids but nevertheless it is worth trying to design an air-based collector for specific applications despite this drawback. Moreover, as insulation is closely linked to solar collector performance use of solar evacuated tube then makes sense in cold climates to reduce heat losses in winter when the heating demand is highest.

Hence, a new kind of solar evacuated tube collector using air as the working fluid is currently developed by Technology of Energy and Energy Efficiency Research Chair (t3e) of École de technologie supérieure (ETS) in Montréal, Canada. The design involves tubes that are open at both ends thus allowing “through flow” of fluid from one end to the other. This type of collector is fairly new according to recent reviews. As a starting point, Solar Rating Certification Corporation (SRCC) solar collectors database has been analysed and no collector of this kind is currently certified [3]. Figure 1 schematically presents the geometry of the collector:

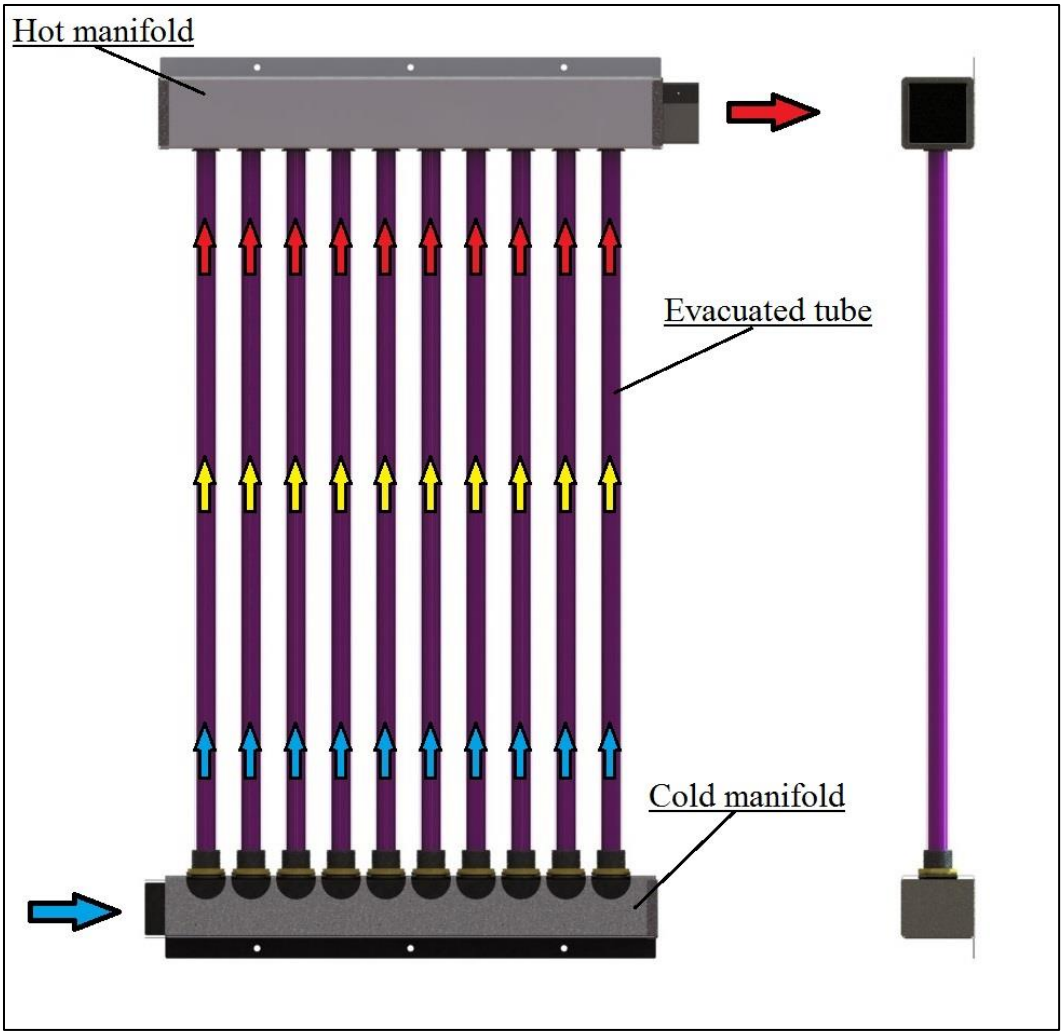

Figure 1 Solar evacuated tube collector using air as the working fluid

In this collector, fresh air from the outside is admitted at the bottom in a cold uninsulated manifold (bottom left). Air rises up within the evacuated tubes, collects heat by convection from the hot inner wall, reaches the hot insulated manifold and is extracted by the fan (top right). In order to evaluate and optimize the performances of this solar collector, a thermal model has been developed. Based on the assumption of an equally distributed mass flow rate in each tube, the global thermal performance of the collector could be estimated analysing the heat transfer phenomena for a single tube.

This paper first presents a brief literature review on the actual technology and the previous thermal models developed. Then, a transient thermal model for a single evacuated tube opened at both ends is developed. The model is then used to predict the performance of the tube as a function of time, airflow rate through the tube, solar radiation, wind speed and ambient temperature. Furthermore, the experimental setup developed to validate the model is presented. The experimental data are compared with

the numerical results. Finally, steady state results are also given in order to evaluate the performances of the tube in a wide variety of environmental and operating conditions.

2. LITTERATURE REVIEW

Solar evacuated tubes thermal collector using air as the working fluid has been used for the first time at the end of the 70's. After the oil crisis of 1973, lots of research work was conducted to find alternate solutions to the use of oil. Solar thermal was considered part of the solution. Figure 2 shows a representation of the collector of Owens-Illinois patented in 1976 [4] and 1980 [5].

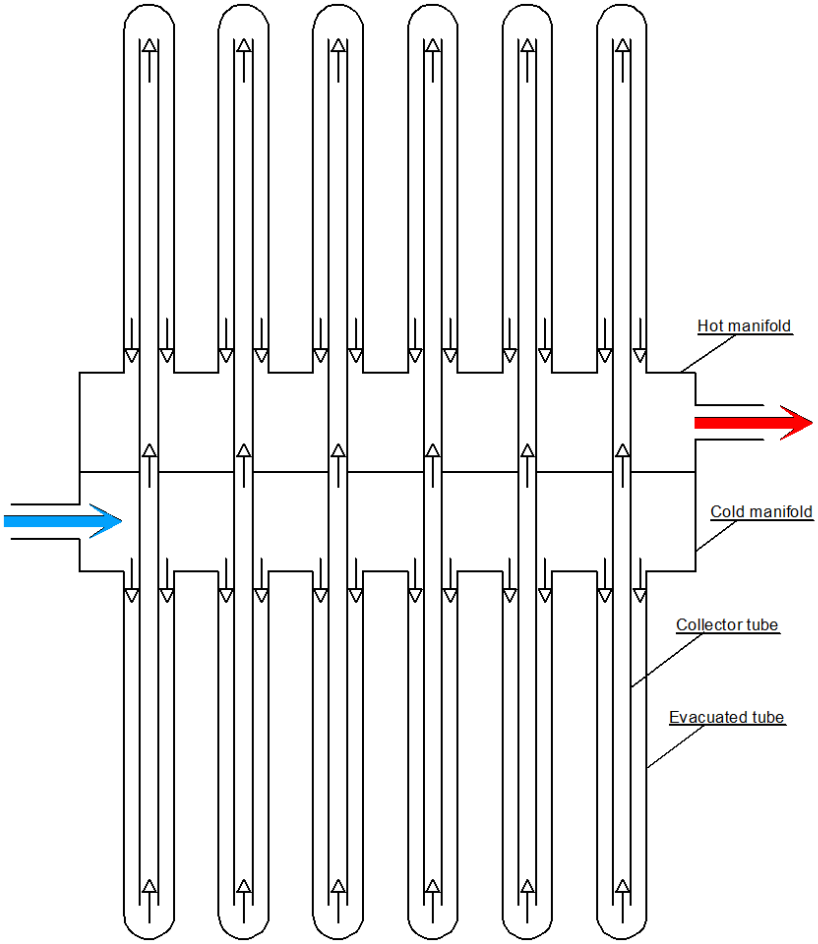

Figure 2 Owens-Illinois solar thermal air collector

On the preceding diagram, there are 12 tubes, in a series/parallel arrangement (6 parallel arrangements of 2 tubes in series). In this collector, outside air is admitted in a cold manifold. Air then goes down heating in contact with the inner wall of the tubes then goes up in an aluminium collector tube. Finally, air flows in a second evacuated tube and

reaches the hot manifold. The arrows on the diagram indicate the direction of the air flow. This collector geometry was first analysed by Eberlein [6]. He developed a one dimensional model to analyse the performances of the collector. The one dimensional approach is also used on similar geometries [7-10]. Kumar, et al. [8] and Bansal and Sharma [9] worked on four types of solar tubes respectively with and without vacuum and with and without selective absorber coating in order to determine the influence of vacuum and coating on the performances. Kim, et al. [7] present a collector tube filled with a water/glycol mixture used as a liquid film to transfer the heat from the receiver to a first aluminium tube into which flows the working fluid flowing upward. This tube is the external shell of a coaxial conduit into which flows the working fluid first downward in the inner tube and then upward. Finally, a German company has also recently worked on this type of collector [11].

The large pressure drop caused by 180° changes in the direction of the air at the bottom of evacuated tubes called for a new design to reduce fan and/or pumping power. This design involves evacuated tubes opened at both ends such as the design proposed in this paper. One particular difference involved in [12] is that the collector involves two insulated manifolds. This makes this collector perfectly symmetric: it permits to direct the flow in either way.

Although work have previously been done to evaluate and optimise the performance of evacuated tubes [7-10], only few published papers [13, 14] have been found on newly commercialised solar evacuated tubes open at both ends and available on the Chinese market. The purpose of this work is then to propose a yet simple but validated model to qualify the heat exchanges occurring in this kind of tube without traditional costly multidimensional CFD simulations.

3. THERMAL MODEL

The thermal model was developed with a step-by-step procedure. A steady state model of the tube in stagnation (without flow) was first developed. The equilibrium temperatures (for the inner and outer glass walls called receiver, r, and cover, c, in the remainder of this work) were obtained from a balance between net gain by radiation and combined convective and radiative losses. This first model involved a simple thermal resistance network for the whole tube. The model was tested against experimental results. It is worth mentioning that for very high radiative fluxes, the temperature of the receiver reached temperatures above 100 °C and one of the tubes exploded due to the high thermal stresses induced by the temperature difference between the cover and receiver welded together.

Then, the model has been modified to take into account unsteady conditions of solar radiation, wind speed and outside air temperature [15]. This problem readily became more involving as the resistance network representation was no longer valid. Nevertheless, the equations were retained and new resistances were calculated from one time step to the next to account for variations with time until convergence. An explicit scheme was implemented that is no updates of coefficients (resistances) were required within a time step. In the third step, a model involving steady-state conditions with fluid flow was elaborated. Hence, as the fluid gained energy, its temperature was increasing along the axis and energy balances were introduced for *n* discrete slices of the tube. Finally, in order to validate the model in real environmental conditions, the model has been extended for unsteady conditions of mass flow rate, solar radiation, wind speed and outside ambient temperature.

In each of those models, the heat transfer is considered one-dimensional along the radial coordinate and axisymmetric. That is there is only one temperature which characterises the inner and outer glass walls, respectively: for a given axial position, heat is equally distributed azimuthally on the receiver and the cover. Moreover, the conduction resistances in the glass walls are considered negligible: there is only one temperature that characterizes the inner and outer surface and the temperature varies axially essentially because of the heat gained by the fluid. As the walls are thin this makes conduction essentially negligible. All data for variable thermal properties with air temperature are readily available to account for such variations [16].

Figure 3 gives a schematic representation and the control volume used along the longitudinal axis of the tube (left). Furthermore, a representation using the thermal/electrical analogy is used to show the radial heat transfer phenomena taking place for a given slice *j* of the tube.

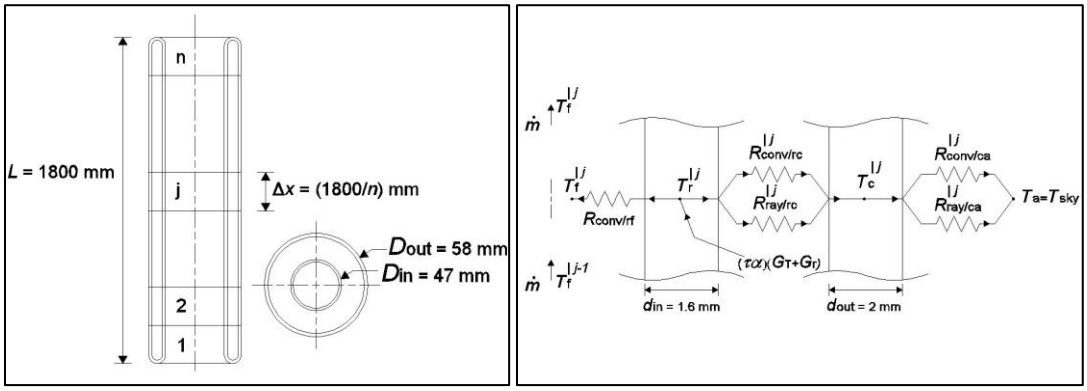

Figure 3 Representation of the tube (left) and the thermal model (right) involving the fluid, the inner (receiver) and outer (cover) glass walls, and the environment.

With respect to the above-mentioned assumptions a unique temperature is used to define the cover temperature (outer glass tube wall) T_c, and the receiver temperature (inner glass tube wall) T_r. Finally, T_f is the mean temperature of the fluid for a given node j.

To solve for the three unknown (T_c, T_r and T_f), three independent equations are written for each control volume of the tube along the longitudinal coordinate. According to the first law of thermodynamic and from Figure 3, we have for the fluid involved in c.v. j:

$$\underbrace{\left(\frac{m_f c_{p/f}^{|j}}{n}\right)\frac{dT_f^{|j}}{dt}}_{\text{Energy stored in the c.v.}} = \underbrace{\rho_f^{|j-1}\dot{V}_f c_{p/f}^{|j-1} T_f^{|j-1}}_{\text{Energy entering the c.v.from the previous node}} + \underbrace{\left[\frac{1}{R_{conv/rf}^{|j}}\right]\left(T_r^{|j} - T_f^{|j}\right)}_{\text{Energy leaving the c.v. in convective heat transfer from the receiver to the fluid}} - \underbrace{\rho_f^{|j}\dot{V}_f c_{p/f}^{|j} T_f^{|j}}_{\text{Energy leaving the c.v. to the next node}} \quad (1)$$

Eq.1 states that the variation of the fluid temperature for a particular slice of fluid is related to the rate of energy transfer that penetrates this c.v. from the previous c.v. and the wall minus the rate of energy transfer that leaves this same c.v. to the next by the mass flow rate. In eq.1, "$R_{conv/rf}$" is the convection resistance between the receiver and the fluid. This resistance is evaluated for each node as a function of fluid temperature and flow regime. The convective heat transfer coefficient needed to determine this thermal resistance is obtained by use of three different correlations according to the flow regime (laminar, transition or turbulent) provided in standard textbooks such as that of Incropera, et al. [16]. The Nusselt number for a constant heat flux at the boundary is used for Reynolds number below 2300, then the Gnielinski correlation is employed for $3000 < Re < 10\,000$ while the Dittus Boelter correlation is used for $Re > 10\,000$. The transition between each correlation is smoothed with a linear interpolation to cover the full range of the Reynolds numbers involved.

For the receiver (the inner glass wall involving the absorption coating) in slice j:

$$\underbrace{\left(\frac{m_{g/in} c_{p/g}}{n}\right)\frac{dT_r^{|j}}{dt}}_{\text{Energy stored in the c.v.}} = \underbrace{(\tau_c \alpha_r)\left(G_T + G_r\right) D_{in}\frac{L}{n}}_{\text{Energy entering the c.v. from solar radiation}} - \underbrace{\left[\frac{R_{conv/rc}^{|j} + R_{ray/rc}^{|j}}{R_{conv/rc}^{|j} R_{ray/rc}^{|j}}\right]\left(T_r^{|j} - T_c^{|j}\right)}_{\text{Energy leaving the c.v. in convective and radiative heat transfer from the receiver tube to the cover tube}} - \underbrace{\left[\frac{1}{R_{conv/rf}^{|j}}\right]\left(T_r^{|j} - T_f^{|j}\right)}_{\text{Energy leaving the c.v. in convective heat transfer to the fluid}} \quad (2)$$

Eq.2 simply states the variation of the receiver temperature is proportional to the net amount of energy absorbed by the receiver minus the heat losses to the cover and to the fluid. In Eq.2, "(τα)" is the standard effective absorptivity-transmissivity couple provided by Duffie and Beckman [17]. It accounts for the transmissivity of the cover and the absorptivity of the receiver. The thermal resistances are again given by Incropera, et al. [16]. "$R_{conv/rc}$" is the convection resistance between the receiver and the cover (in the

vacuum annular space). In the original work proposed by Eberlein in 1976, this resistance was completely neglected assuming perfect vacuum. Here, the assumption of continuous medium does not hold and using an "effective convective heat transfer coefficient" in a partial vacuum may be hazardous. Nevertheless, several values of effective heat transfer coefficient were used without significant changes into solutions. "$R_{ray/rc}$" is the radiative resistance between the receiver and the cover. The long infinite cylinder approximation [16] is used to evaluate this resistance although the tube is discretized into small slices along the longitudinal axis (view factors – and hence radiative coupling – between slices is not considered).

Finally, for the cover in slice *j*:

$$\underbrace{\left(\frac{m_{g/out}c_{p/g}}{n}\right)\frac{dT_c^{|j}}{dt}}_{\text{Energy stored in the c.v.}} = \underbrace{\left[\frac{R_{conv/rc}^{|j}+R_{ray/rc}^{|j}}{R_{conv/rc}^{|j}R_{ray/rc}^{|j}}\right]\left(T_r^{|j}-T_c^{|j}\right)}_{\text{Energy entering the c.v. in convective and radiative heat transfer from the receiver tube to the cover tube}} - \underbrace{\left[\frac{R_{conv/ca}^{|j}+R_{ray/ca}^{|j}}{R_{conv/ca}^{|j}R_{ray/ca}^{|j}}\right]\left(T_c^{|j}-T_a\right)}_{\text{Energy leaving the c.v. in convective and radiative heat transfer from the cover tube to the ambient}} \quad (3)$$

Eq.3 states that the change in cover temperature is proportional to the difference between the net heat rate from the receiver and the losses to the environment. "$R_{ray/rc}$" is calculated based upon several assumptions: the transmissivity of the cover is 0.95 for radiation coming from the sun and the environment while the reflectivity is 0.05 meaning that absorption is negligible; the absorptivity of the receiver for the same wavelengths is set to 0.95 while the emissivity of the receiver at a longer wavelength is a function of temperature such as described in [18] based on specification of a selective coating manufacturer; the emissivity of both faces of the cover is set to 0.9; the absorptivity of the cover to radiation emitted by the receiver is 1 while the transmissivity is necessarily 0. "$R_{conv/ca}$" is the convective resistance between the cover and the environment. The correlation proposed by Zukauskas for a single tube in a cross flow is implemented to evaluate the convection coefficient with the wind speed supposed perpendicular to the tube. Finally, "$R_{ray/ca}$" is the radiative resistance between the cover and the environment. The approximation of a small object in a large environment of uniform temperature is used. Furthermore, the surrounding radiative temperature is set equal to the ambient temperature as a simplification. Strictly, this should underestimate heat losses for bright and clear days as the effective "sky" temperature T_{sky} would be lower than T_a.

To complete this model, the glass properties are assumed to be constant while the fluid (air) properties inside the tubes and in the environment are function of the temperature. Table 1 shows a brief summary of the parameters used in the model.

Table 1 Numerical value of the parameters used in the model

Parameter	Value	Units
D_{out}	0.058	m
D_{in}	0.047	m
d_{out}	0.002	m
d_{in}	0.0016	m
α_r	95	%
τ_c	95	%
ε_r	4 $0.022T_r$ - 2.37	% for 0 K ≤ T_r ≤ 293 K % for 293 K ≤ T_r ≤ ∞
ε_c	90	%
L	1.8	m
ρ_g	2230	kg/m^3
$c_{p/g}$	837.2	J/kg K
air properties	function of T_f	using Incropera, et al. [16] data

Using the environmental parameters (solar radiation, wind speed, ambient temperature) and the operating parameter (airflow) as input parameters for the model, it's possible to simulate the outlet air temperature in transient conditions. A fourth order Runge-Kutta method is used to solve the time derivatives. Figure 4 shows the resolution algorithm implemented in Matlab.

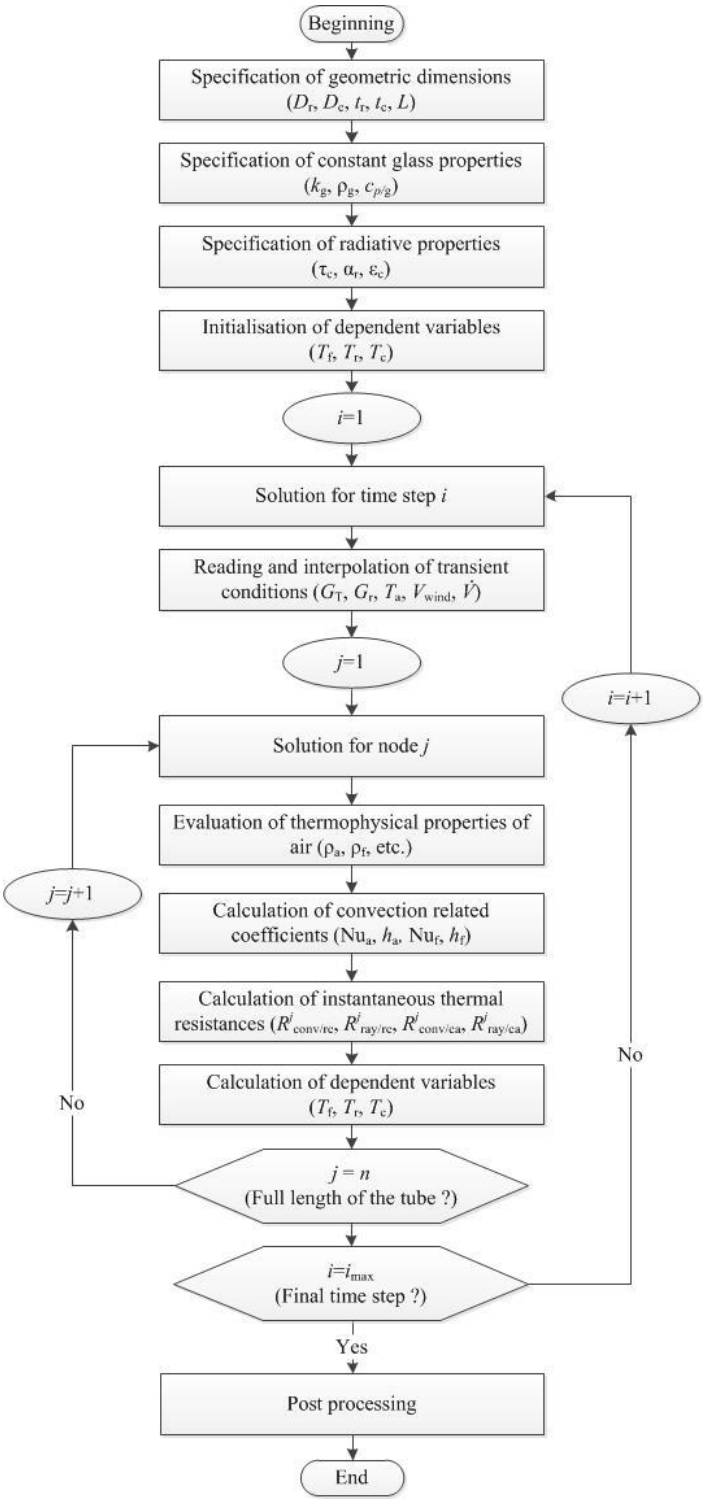

Figure 4 Resolution algorithm implemented in Matlab

The next section presents the experimental setup and the necessary instrumentation required to validate the proposed model.

4. EXPERIMENTAL SETUP

A weather station is used to measure environmental parameters. Wind speed is measured with a RMY05103L wind monitor from RM Young. The anemometer provides wind speed with approximately ± 0.3 m/s accuracy (the wind direction is not taken into account in the model although the Zukauskas correlation is for a tube in a cross flow). The incident solar radiations, total and reflected, are measured with CMP3 pyranometers from Kipp & Zonen with accuracy below 10 % in average on a full day. Finally, the ambient temperature is measured with a QFA3171 RTD PT1000 temperature sensor from Siemens including a radiation shield. The accuracy of the temperature measurement is approximately ± 0.8 K for the full range of the sensor. An evacuated tube open at both ends was installed on a mounting rack outside on the roof of École de technologie supérieure in Montréal, Canada. The tube was tilted at an angle of 45 ° and oriented in the plane of the north-south azimuth. The experimental setup and an identification of the principal components are presented in Figure 5 (left) and a picture of the real bench test (right).

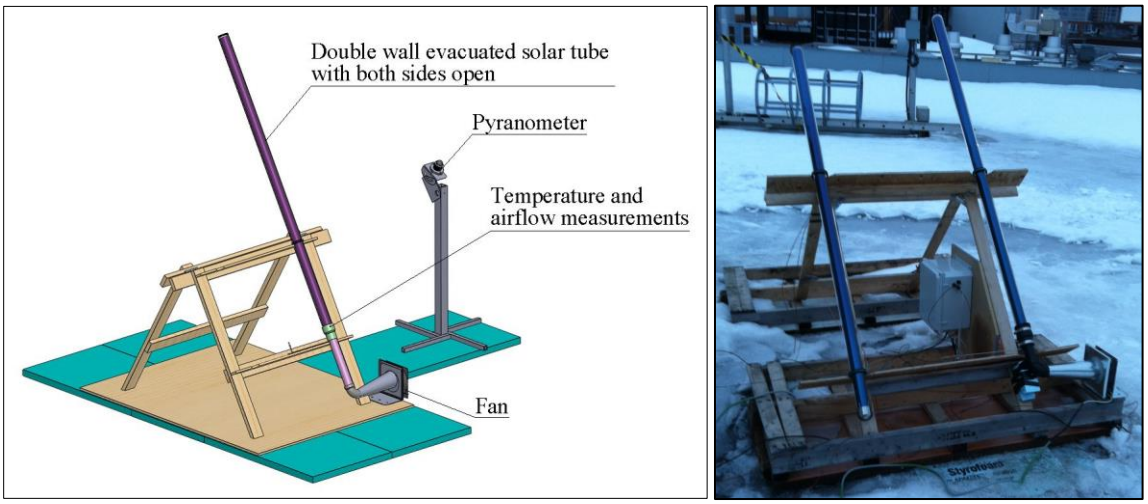

Figure 5 Experimental setup, schematic and identification of the component (left) real bench test (right)

A pitot tube is used to determine the airflow rate. In fact, the pitot tube measures the dynamic pressure "P_{dyn}" using a pressure transducer having an approximate precision of ± 0.2 Pa. Since the pressure transducer is located outside, a heated enclosure was designed to protect it against cold temperatures that could impair the measurement. The velocity is obtained with the following relation:

$$P_{dyn} = 0.9 \times \frac{1}{2} \rho_f u_f^2 \quad (4)$$

The 0.9 factor is a correction factor used to take into account the velocity profile in the tube as the measurement is taken in the center of the tube section where the velocity is maximum. The measured velocity is corrected with the measured temperature since "ρ_f" varies with temperature. The temperatures were measured with a calibrated special class type T thermocouple having a precision of ± 0.5 °C.

It is worth noting that as the airflow rate increases, the precision in the measurement of air flow velocity is better. However, on the contrary, the temperature gain, ΔT, throughout the tube is reduced and the precision on the temperature measurement is also reduced. Hence, a balance in the operating parameters of the validation experimental setup needs to be achieved to guarantee an acceptable range of precision in the measurements.

Preliminary simulations with the model have been carried out to predict the performances of the tube and propose an adequate mass flow rate and temperature gain tandem. On a sunny day, a temperature increase of about 10 °C throughout the tube is achieved with a volumetric air flow rate of about 30 m^3/h (air velocity, u_f around 5 m/s). This set of operating parameters provides a good compromise on the precision of both the air flow rate determination and the temperature measurement of the air leaving the tube.

5. VALIDATION

Figure 6 presents a comparison of experimental results and predictions for a bright sunny day. The measurements are carried out around solar noon to reduce the sensibility of the measurement made with a fixed pyranometer in the plane of the collector (Figure 5). The simulation presented in Figure 6 involved results obtained with only 3 nodes which give a good compromise between the precision of the solution and calculation time. A time step of 0.01 second was used to respect the CFL criterion. Results for several days were compared to assess the validity of the predictions over a period of four months.

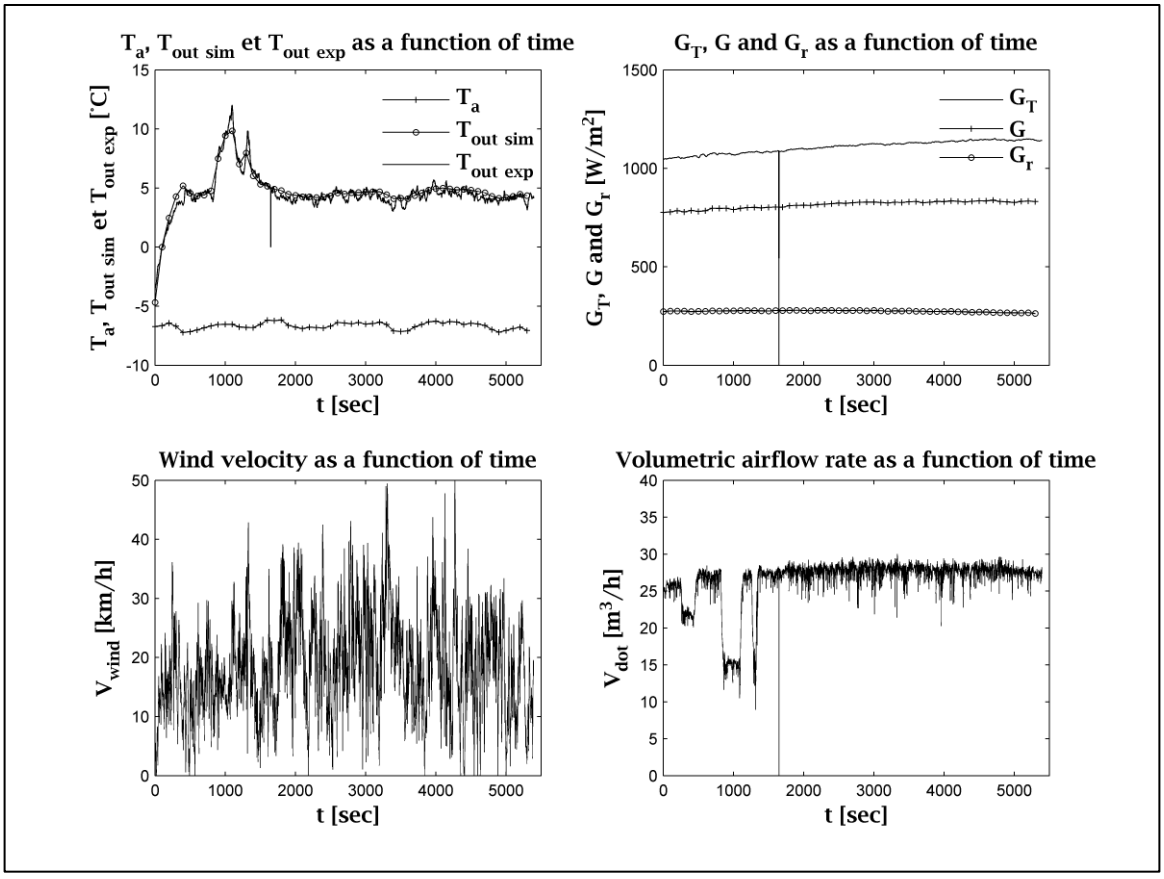

Figure 6 Validation of the model with experimental results

Figure 6 presents four graphs, the upper left one shows the outlet air temperature (experimental data and simulated one) and the ambient temperature. On the upper right graph the three measured solar radiations are shown. G_T is measured in the plane of the tube, G is the total horizontal solar radiation and G_r is the reflected solar radiation. G is not used explicitly as an input for the simulation model, but the information was available from the weather station and is given here as a piece of additional information. The wind speed is presented on the third lower left graph. Finally, the volumetric airflow rate is shown on the last graph (lower right corner). The mean value is around 30 m^3/h and variations have been manually induced to test the transient behavior of the model (the flow was reduced to about 15 m^3/h). Some noise is present on the airflow rate measurement. This noise is due to the wind. In fact, as the dynamic pressure is measured to obtain the airflow rate indirectly, and the end of the tube is open to ambient air, the wind necessarily influences this measurement. All graphs involve a reading error at about 1700 s where the system sent back a 0 value. Figure 7 focusses specifically the comparison between predicted outlet air temperatures and experimentally measured one.

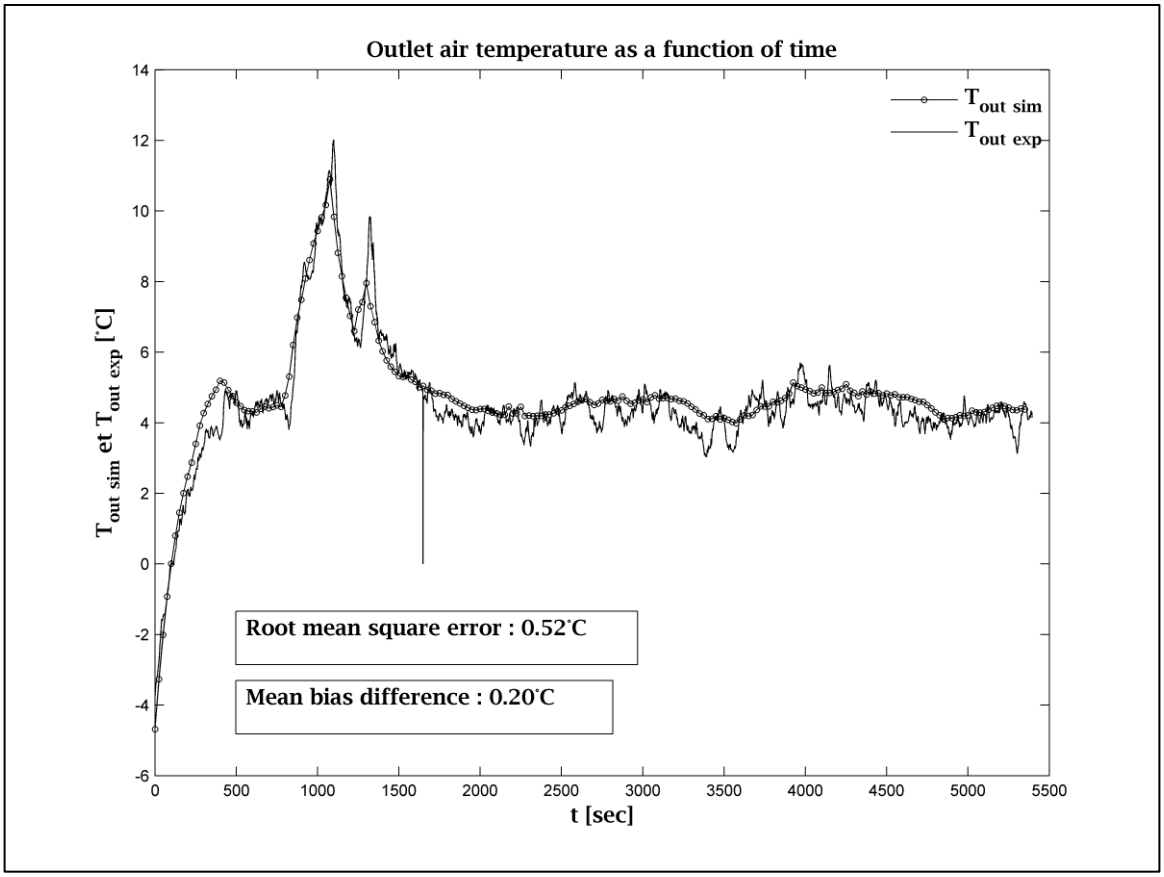

Figure 7 Simulated and measured outlet air temperature comparison

Although the model doesn't exhibit the rapid variations of temperature (probably caused by the turbulence of the flow), the numerical model (dotted line) follows very well the experimental (continuous line) behavior of the tube. Two statistical indicators are also calculated two qualify the difference between the results. A root mean square error of 0.52 °C and a mean bias difference of 0.20 °C are then obtained. Since the gain in temperature is around 10 °C a difference of 0.52 °C is in the range of the precision of the type T thermocouple but in general the model overestimates the outlet temperature of 0.20 °C. Moreover, this could be explained by the assumption that $T_a = T_{sky}$ in the model which slightly reduces the heat losses to the environment. Finally, the precision of the velocity (pressure) sensors, the experimental uncertainty and the correlations used to determine the convection coefficient may explain the differences.

With a validated model, it is possible to analyse the influence of the environmental conditions (ambient temperature, wind speed, solar radiation) and operation (airflow) parameters on the performances of the tube using this transient model in steady state.

6. STEADY STATE PREDICTIONS

The preceding model (Eqs.1-3) can be solved in steady state. In this case, the energy storage term becomes 0 and the Runge-Kutta method is no longer needed. In fact, in steady state a simple linear system of equation is obtained that can be solved for the three unknown temperatures at each node *j*. Matlab matrix inversion capabilities are conveniently used to realise this. Initial values of the coefficients are used since these coefficients (the thermal resistances) depend on the final solution (the temperature at each node). Hence, the linear system of equation is solved iteratively. The model is then used to see the impact of different factors used to characterise the performances of the tube: outlet air temperature, T_{out}, mean global heat transfer coefficient (inside the tube), HTC, thermal efficiency, η, and the pressure drop, ΔP. The pressure drop is calculated using the Colebrook correlations [19]. The thermal efficiency is defined according to the following equation:

$$\eta = \frac{\dot{Q}_{\text{useful}}}{G_T A} \times 100\% \tag{5}$$

Where $\dot{Q}_{\text{useful}}$ is defined as:

$$\dot{Q}_{\text{useful}} = \dot{m}(c_{p/\text{outlet}} T_{\text{outlet}} - c_{p/\text{inlet}} T_{\text{inlet}}) \tag{6}$$

Eq.5 is a standard expression but here the definition of the surface area, *A*, is important to specify. As a single tube is investigated, *A* is based upon the external diameter of the outside tube (cover), D_{out}. Strictly, this would mean that a multi tubes collector would involve no spacing between tubes which is usually not the case. This implies that rather large efficiencies are expected for the single tube.

Figure 8 shows the influence of solar radiation G_T on T_{out}, HTC, η, and ΔP with T_a = 20 °C, V_{wind} = 5 km/h, and $\dot{V}$ = 30 m^3/h. Spatial discretization was performed with 100 nodes located every 1.8 cm along the tube. The mesh independency of the solution has been verified and no significant differences have been identified above 10 nodes.

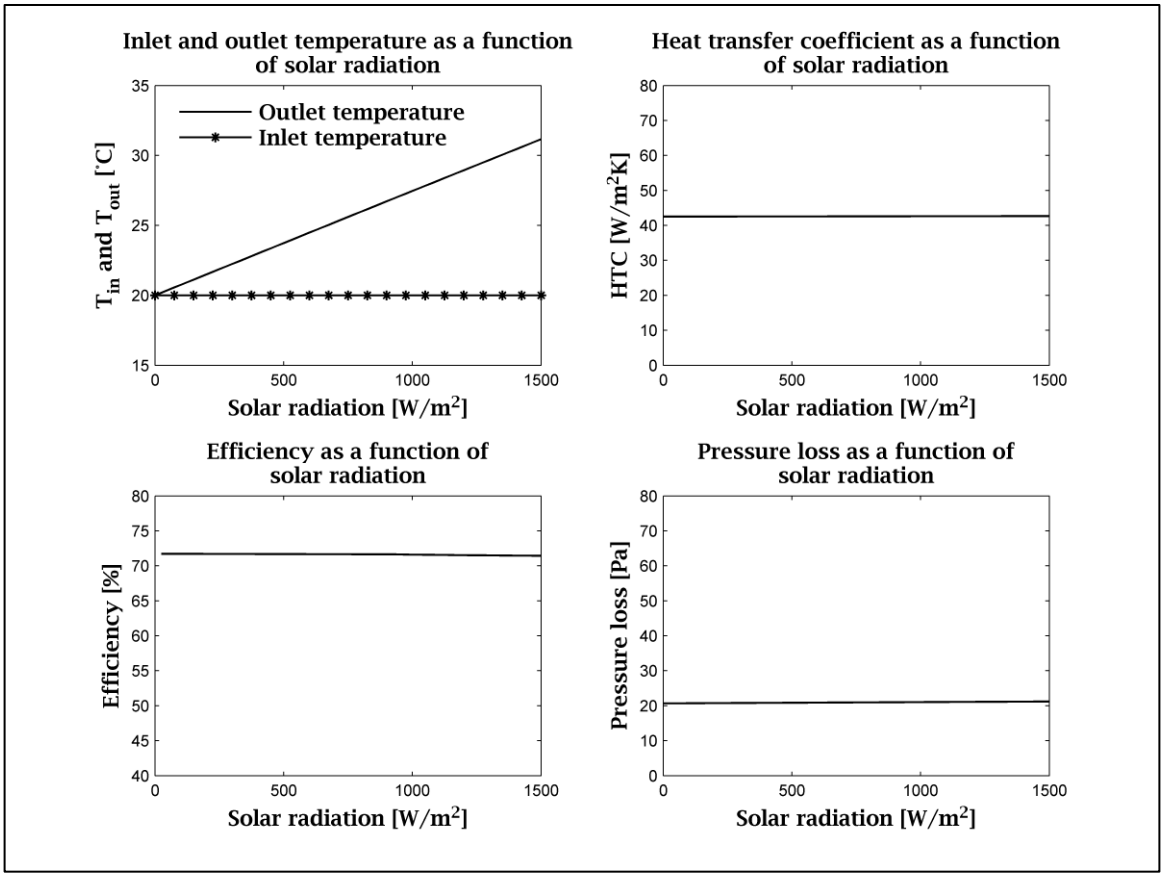

Figure 8 Influence of solar radiation G_T [W/m^2] on T_{out} [°C], HTC [W/m^{2}K], η, and ΔP [Pa] (T_a = 20 °C, V_{wind} = 5 km/h, and $\dot{V}$ = 30 m^3/h)

Figure 8 presents four graphs, the upper left one shows the influence of solar radiation on the outlet temperature. On the upper right graph the heat transfer coefficient as a function of the solar radiation is presented. Influence on efficiency is also presented on the third lower left graph. Finally, the impact on pressure drop is shown on the last graph (lower right corner). All following figures are constructed as such.

These results show a negligible influence of solar radiation on the pressure drop, efficiency and heat transfer coefficient. Pressure drop and HTC variations are simply due to variations in thermophysical properties. Efficiency calculations based on the projected surface area of the tube imply that the losses in efficiency are mainly due to the solar radiation reflected by the cover, the losses by the cover by radiation and convection and the geometrical loss due to the fact that the inner tube as a smaller diameter than the outer tube. As the convective losses are nearly constant for the range of temperature variations considered here, the efficiency is nearly constant decreasing about 2% with the increase of G_T. Hence, with a nearly constant η, the temperature increase with G_T is nearly linear as shown in the upper left graph. The outlet temperature is identical to the ambient temperature when there is no solar radiation and the efficiency drops to 0. The outlet air

temperature increases almost linearly with the augmentation of solar radiation to attain an augmentation of 11.2 °C over the ambient temperature at 1500 W/m^2 of solar radiation. The more the source term (Eq.2) increases, the more the fluid will absorb energy.

Figure 9 shows the influence of the ambient temperature T_a on the above mentioned parameters with G_T =1000 W/m^2, V_{wind} = 5 km/h, and $\dot{V}$ = 30 m^3/h.

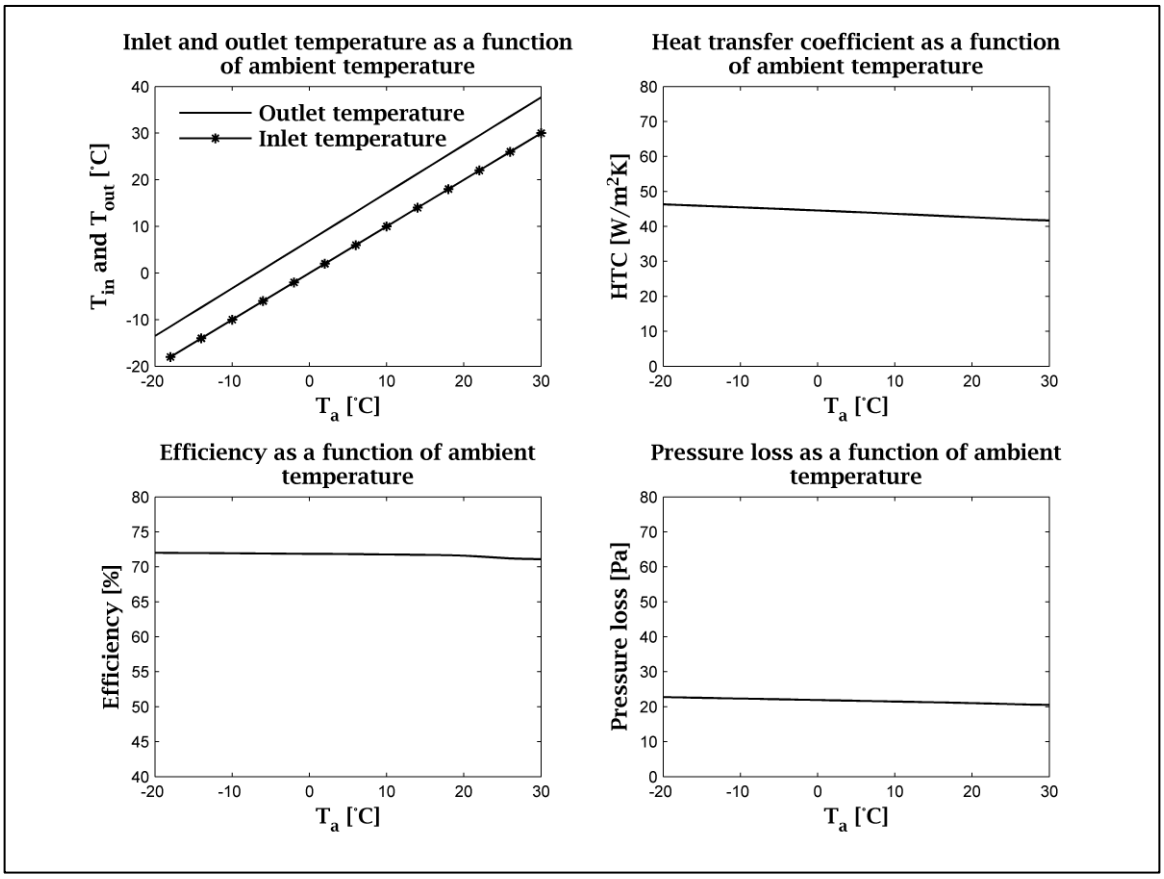

Figure 9 Influence of ambient temperature T_a [°C] on T_{out} [°C], HTC [W/m^{2}K], η, and ΔP [Pa] (G_T = 1000 W/m^2, V_{wind} = 5 km/h, and $\dot{V}$ = 30 m^3/h)

Figure 9 indicates that the influence of the ambient temperature is not much more important than that of the solar radiation on heat transfer coefficient, pressure loss and efficiency. Since the airflow rate in the tube is high (30 m^3/h is equivalent to a turbulent flow, Re=16 250), the convective heat transfer to the circulating fluid is good. As a consequence, the receiver temperature is maintained at a reasonable temperature relatively to the ambient temperature and the heat losses by both radial convection and radiation from the cover tube to the ambient are low. This is the main reason why the efficiency is almost independent of the ambient temperature and the solar radiation. The pressure loss is reduced as the ambient temperature rise because the viscosity is reduced with the temperature. Similarly, the heat transfer coefficient is reduced as the ambient

temperature rises. This overall decay of HTC is due to the combination of the variation of density, viscosity, thermal diffusivity, mass flow rate and consequently that of Re, Pr, and Nu. For instance, the density falls with increasing temperature and proportionally the mass airflow rate as the volumetric airflow rate is fixed.

Figure 10 shows the influence of the wind speed V_{wind} [km/h] on the above mentioned parameters with G_T =1000 W/m^2, T_a =20 °C, and $\dot{V}$ = 30 m^3/h.

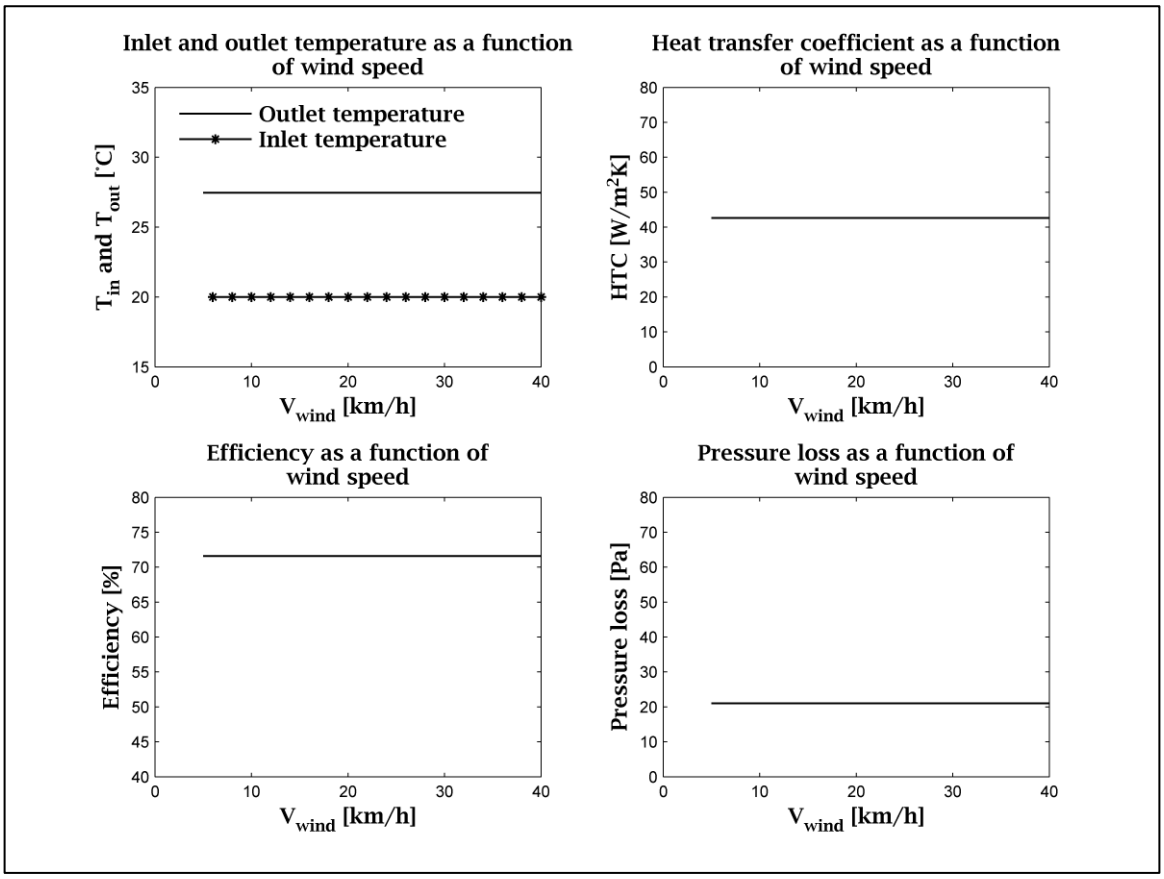

Figure 10 Influence of wind speed V_{wind} [km/h] on T_{out} [°C], HTC [W/m^{2}K], η, and ΔP [Pa] (G_T = 1000 W/m^2, T_a =20 °C, and $\dot{V}$ = 30 m^3/h)

Figure 10 indicates that wind as practically no influence on any of the performances criteria analysed because despite a variable external heat transfer coefficient with wind speed, the total external resistance is driven by radiation due to the great insulation provided by the vacuum annular space between the outer (cover) and inner (receiver) tubes.

Finally, Figure 11 shows the influence of the volumetric airflow rate $\dot{V}$ on T_{out}, HTC, η, and ΔP with T_a = 20 °C, V_{wind} = 5 km/h, and G_T = 1000 W/m^2. 100 nodes were still used.

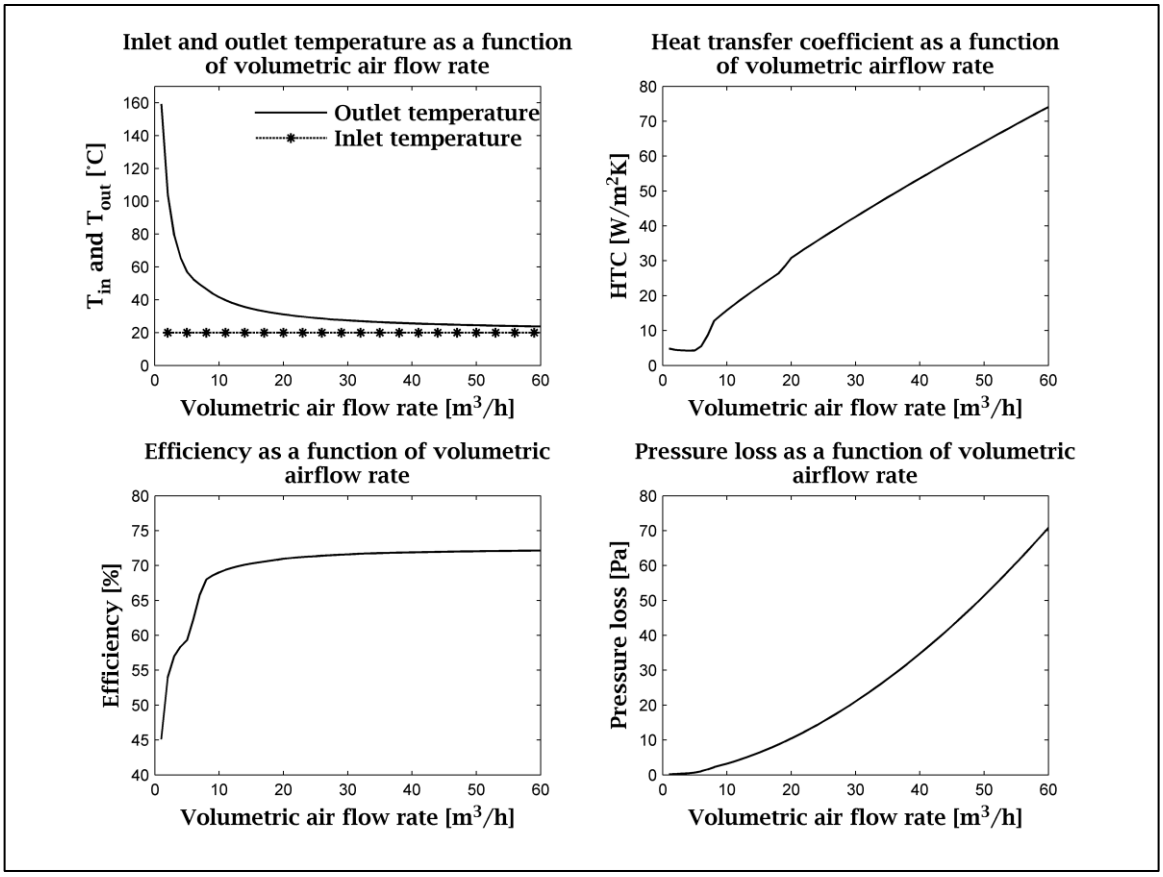

Figure 11 Influence of the volumetric airflow rate $\dot{V}$ [m^3/h] on T_{out} [°C], HTC [W/m^{2}K], η, and ΔP [Pa] (T_a = 20 °C, V_{wind} = 5 km/h, and G_T = 1000 W/m^2)

Figure 11 shows the strong influence of the inner volumetric air flow rate on the performances of the tube double-walled tube. As specified by Delisle and Kummert [20] the influence of the flow rate is of primary importance in air collector. For small flow rates a temperature gain above 100 °C can be obtained. But in this case, the efficiency is quite low due to higher heat loss of the evacuated tube to the surrounding by radiation and convection. As the airflow rate increases, the temperature gain goes down to almost 0 (above 40 m^3/h) and the efficiency reaches about 70 %. As the thermal losses reduce to almost zero with a high flow rate and constant optical losses (radiative properties are considered independent of T), this explains why the maximum efficiency asymptotically tends to 70 % with low convective losses. Naturally, as the flow rate increases, the pressure drop increases too as it usually varies with the square of the fluid velocity. Finally, there is three different sections for the convective heat transfer coefficient to the heat transfer fluid (one for each flow regime: laminar, transition, turbulent) due to the use of three different correlation (on for each of the flow regime). This explains the somewhat irregular shape of the curve for HTC.

7. CONCLUSION

This work presents a new design of thermal solar collector using air as the working fluid and evacuated tubes opened at both ends as the basic component. This solar collector is intended to provide the best performances in cold climates. A simple axisymmetric 1D model of the heat exchanges taking place in a single evacuated solar tube is presented and experimental validation results are provided. A good agreement between the simulations and the experimental measurements is found: a root mean square error of 0.52 °C is calculated on the outlet airflow temperature, T_{out}.

Finally, the steady state model is used to explore the impact of the weather – solar radiation G_T [W/m^2], ambient temperature T_a[°C], and wind velocity V_{wind} [km/h] – and operation parameter – volumetric air flow rate $\dot{V}$ [m^3/h] – on different performance indicators (outlet temperature T_{out} [°C], heat transfer coefficient HTC [W/m^{2}K], efficiency η, and pressure drop ΔP [Pa]). The volumetric airflow rate is shown to be the parameter with the most influence on the performances.

This suggests that collectors should be designed with the maximum airflow rate to ensure the maximum efficiency while respecting the constraint of the minimum temperature gain required by the process, if any.

Future of work should include the development of tubes that could sustain the constraints caused by the thermal expansion of the hot inner tube (receiver) for very low or no airflow.

ACKNOWLEDMENT

First author acknowledge the Natural Sciences and Engineering Research Council of Canada (NSERC) for Alexander Graham Bell scholarship and Fonds de recherche du Québec – Nature et technologies and Ecosystem for support. The authors also thank the partners of the t3e research chair who support the project.

RERERENCES

[1] Ressources naturelles Canada, Energy Efficiency Trends in Canada 1990 to 2009, in, 2011.

[2] A. Moreau, F. Laurencelle, Performance des chauffe-eau solaires installés au Québec dans le cadre du projet pilote sur les chauffe-eau solaires domestiques du Bureau de l'efficacité et de l'innovation énergétiques – rapport final, in, Bureau de l'efficacité et de l'innovation énergétiques, 2012.

[3] SRCC, 2011, Ratings Summary Page,< https://secure.solar-rating.org/Certification/Ratings/RatingsSummaryPage.aspx >. Consulté le 2013-07-10.

[4] K. L. Moan, Tubular solar energy collection system utilizing air media, in, L. Moan, Kenneth, État-Unis, 1976.
[5] H.E. Novinger, Low profile evacuated-bottle solar collector module, in, Novinger, Harry E., État-Unis, 1980.
[6] M.B. Eberlein, Analysis and Performance Predictions of Evacuated Tubular Solar Collectors Using Air as the Working Fluid, University of Wisconsin, 1976.
[7] J.T. Kim, H.T. Ahn, H. Han, H.T. Kim, W. Chun, The performance simulation of all-glass vacuum tubes with coaxial fluid conduit, International Communications in Heat and Mass Transfer, 34 (2007) 587-597.
[8] R. Kumar, S.C. Kaushik, H.P. Garg, Transient analysis of evacuated tubular solar collector with finite difference technique, Renewable Energy, 4 (1994) 941-947.
[9] N. Bansal, A. Sharma, Transit theory of a tubular solar energy collector, Solar energy, 32 (1984) 67-74.
[10] H. Liang, Experimental research on the all-glass evacuated tube solar air collector, in: D.Y. Goswami, Y. Zhao (Eds.) Proceedings of ISES World Congress 2007 (Vol. I – Vol. V), Springer Berlin Heidelberg, 2009, pp. 674-677.
[11] Kollektorfabrik, 2012, Sun Storm,< http://www.kollektorfabrik.de/ >. Consulté le 17 juillet 2013.
[12] Airwasol, 2013, Solar technologies,< http://www.airwasol.de/ >. Consulté le 17 juillet 2013.
[13] L.J. Shah, S. Furbo, Vertical evacuated tubular-collectors utilizing solar radiation from all directions, Applied Energy, 78 (2004) 371-395.
[14] L.J. Shah, S. Furbo, Modeling shadows on evacuated tubular collectors with cylindrical absorbers, TRANSACTIONS-AMERICAN SOCIETY OF MECHANICAL ENGINEERS JOURNAL OF SOLAR ENERGY ENGINEERING, 127 (2005) 333.
[15] P.-L. Paradis, S. Hallé, G. Quesada Ramos, D. R. Rousse, L. Guillon, Modèle thermique d'un tube sous vide en stagnation, in: AMT 2014, Agadir, Maroc, 2014.
[16] F.P. Incropera, A.S. Lavine, D.P. DeWitt, Fundamentals of heat and mass transfer, John Wiley & Sons Incorporated, 2011.
[17] J.A. Duffie, W.A. Beckman, Solar engineering of thermal processes, John Wiley & Sons, Inc., New Jersey, 2006.
[18] ALMECO solar, 2013, Tinox tube 2.0,< http://www.almecosolar.com/Brochure/tinox_tube_en.pdf >. Consulté le 10 décembre 2013.
[19] F.M. White, Fluid mechanics, 7 th ed. ed., McGraw-Hill, New York, 2011.
[20] V. Delisle, M. Kummert, Experimental Study to Characterize the Performance of Combined Photovoltaic/Thermal Air Collectors, J. Sol. Energy Eng, 134 (2012).